

IMPROVING THE WELDABILITY OF FECRAL WELD OVERLAY COATINGS

J.N. DuPont, J.R. Regina, and K. Adams
Lehigh University, Bethlehem, PA 18015

ABSTRACT

Fe-Cr-Al weld claddings are currently being considered as corrosion resistant coatings for boiler tubes in coal fired power plants. Although these alloys could potentially be good coating candidates due to their excellent high-temperature corrosion resistance, they are susceptible to cracking due to hydrogen embrittlement at elevated aluminum concentrations. The current study investigated the hydrogen cracking susceptibility of Fe-Cr-Al weld overlay claddings deposited by the gas tungsten arc and gas metal arc processes. The cracking susceptibility of these alloys is a strong function of the Al and Cr content of weld overlay. Additions of Cr to the overlay will decrease the amount of Al that can be accommodated before cracking occurs. Less Al and Cr could be tolerated in gas metal arc welds compared to gas tungsten arc welds. The hydrogen cracking susceptibility was not linked exclusively to the formation of the inherently brittle intermetallic compounds (Fe_3Al and FeAl) as observed from previous results on Fe-Al weld overlays. The presence of $(\text{Fe,Cr})_x\text{C}_y$ and $(\text{Fe,Al})_3\text{C}$ type carbides was found to improve the cracking resistance to the point where crack-free welds could be obtained on some of the overlays that contained the brittle intermetallic phases. This improvement in cracking resistance is attributed to the hydrogen trapping potential of the carbide phases. Research currently being conducted to exploit the beneficial effect of carbides for reducing cracking susceptibility is described.

INTRODUCTION

Fe-Cr-Al based alloys are good candidates for corrosion resistant weld overlay coatings because they exhibit excellent oxidation and sulfidation resistance in a wide range of high-temperature environments. These alloys rely on both aluminum and chromium additions for increased corrosion protection, and it has been shown that the corrosion resistance of these alloys in simulated low NO_x environments improved with an increase in the aluminum and chromium concentrations. Recent studies have indicated that Fe-Cr-Al based alloys require approximately 7.5 - 10% wt% aluminum and chromium additions up to ~ 5 wt% to remain protective in a wide variety of low NO_x type atmospheres^{1,2}. Unfortunately, these alloys are also susceptible to cracking due to environmental embrittlement from hydrogen. Previous work has shown that Fe-Al weld overlays produced with both the GTAW and GMAW processes were subject to cracking when the aluminum concentration in the weld deposit was greater than approximately 8-11% Al³, and this Al range represents the composition over which the intermetallics begin to form. Thus, the objective of this research is to establish the range of weldable FeCrAl compositions and develop methods for improving the cracking resistance of the coatings so that they can be exploited for corrosion protection in coal fired power plants.

EXPERIMENTAL PROCEDURE

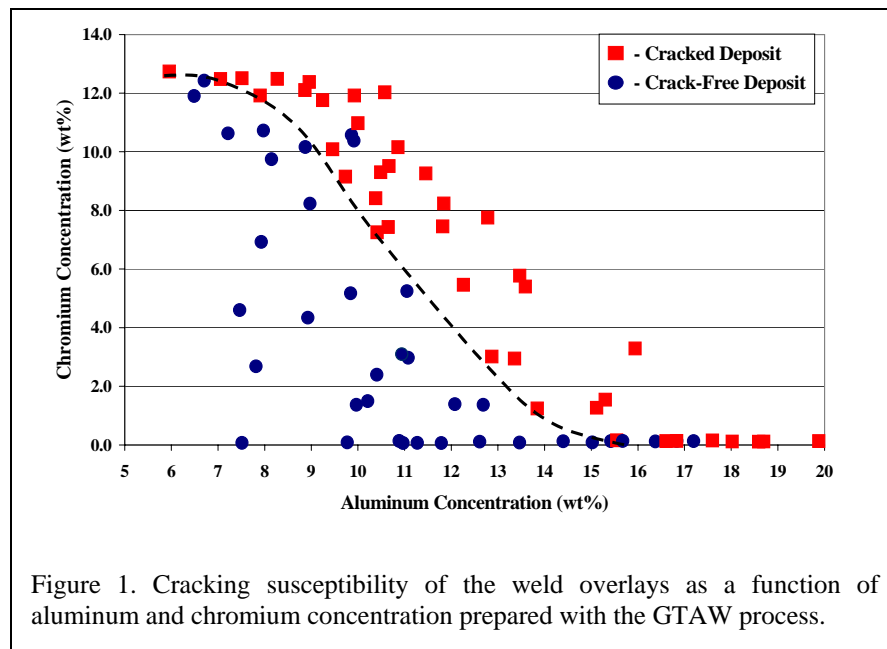
Gas tungsten arc (GTAW) and gas metal arc (GMAW) weld overlays were deposited onto A285C carbon steel (0.16 wt% C). For the GTA welds, a dual wire feeder system was utilized with commercially pure 1100 aluminum and 430 ferritic stainless steel filler metals. A smaller matrix of welds was prepared on a low carbon experimental substrate (0.017 wt% C). Welds with a wide range of aluminum and chromium concentrations were prepared by independently varying the feed rates of the two filler metal wires. Welds were produced with a travel speed of 2mm/s and energy input of approximately 1210J/mm. The filler metal wire feed speeds were independently varied from 0 – 74mm/s to adjust the aluminum and chromium contents of the weld deposits. The GMA welds were prepared with a composite wire that had a solid Al core and a steel outer sheath with Cr powder additions. The cracking behavior of the weld deposits was investigated using a non-destructive dye-penetration technique. Weld overlay compositions were determined using electron probe microanalysis (EPMA). Phase identification was conducted using X-Ray Diffraction (XRD) on a Bruker AXS General Area Detector Diffraction System using $\text{Co K}\alpha$ x-rays. Weld samples were removed in cross-section, mounted, and polished to 0.01 μm SiO_2 finish for light optical microscopy (LOM). Measurements of the particle area fraction and number of particles per unit area of weld were made using a LECO[®] quantitative image analysis (QIA) system interfaced with a light optical microscope. Identification of fine scale carbides was performed by removing the carbide precipitates from the matrix using a

carbide extraction technique. Samples were also prepared with an FeCrAl matrix and various quantities of TiC as hydrogen trapping sites. These alloys were prepared with an arc button melting process using virgin materials.

RESULTS AND DISCUSSION

GTA WELDS

Figure 1 shows the cracking susceptibility of the weld overlays as a function of aluminum and chromium concentration prepared with the GTAW process. The XRD phase identification results are shown in Figure 2. There were four microstructural regimes observed in the weld overlay coatings: ferrite with $(\text{Fe,Al})_3\text{C}$ carbides, ferrite with $(\text{Cr,Fe})_x\text{C}_y$ carbides, $\text{Fe}_3\text{Al}/\text{FeAl}$ with $(\text{Fe,Al})_3\text{C}$ carbides, and $\text{Fe}_3\text{Al}/\text{FeAl}$ with $(\text{Cr,Fe})_x\text{C}_y$ carbides. The weldability boundary from Figure 1 is superimposed on the phase ID results for reference, and the approximate location of the order/disorder transformation boundary that indicates the formation of $\text{Fe}_3\text{Al}/\text{FeAl}$ intermetallic phases is also shown. It was not possible to distinguish between the Fe_3Al and FeAl intermetallic phases, so they are collectively grouped as $\text{Fe}_3\text{Al}/\text{FeAl}$ here. The phase fields containing $\text{Fe}_3\text{Al}/\text{FeAl}$ phases may have also contained ferrite, but due to the peak overlap between these phases it could only be determined that the intermetallic phases were present within the weld metal as a result of the super lattice reflections. Thus, the order/disorder transformation boundary describes the composition range where ferrite phase begins to transform to the ordered intermetallic phases. Chromium additions appeared to moderately stabilize the ferrite phase, as increasing the chromium content of the weld caused the intermetallic transformation to occur at higher aluminum concentrations. According to the binary Fe-Al phase diagram, a two-phase region of ferrite + Fe_3Al has been reported to exist between approximately 11wt%Al – 13wt%Al. From the reported phase diagrams, the actual order/disorder transformation may have occurred over a range of aluminum concentrations, where the onset of the ordered transformation began at approximately 11wt%Al and may not have completely transformed to the ordered intermetallic Fe_3Al phase until approximately 13wt%Al (for binary Fe-Al welds). The $(\text{Fe,Al})_3\text{C}$ carbides form in the weld overlays containing less than 4wt%Cr, whereas welds containing above approximately 4wt%Cr contained the $(\text{Cr,Fe})_x\text{C}_y$ type carbides. Research conducted to date has shown that the hydrogen cracking susceptibility of Fe-Al type alloys is linked exclusively to the presence of the brittle Fe_3Al and FeAl intermetallic phases^{3,4}. However, the combined weldability and phase ID results shown in Figure 2 indicate that the cracking susceptibility of these weld overlays can not be linked solely to the presence of the intermetallic phases. Crack-free welds could be deposited on some compositions that exhibited the intermetallic phases, while cracking was observed on some of the alloys that did not exhibit any of the ordered intermetallic phases. These results indicate that the addition of chromium and the presence of second phase particles has a strong influence on the cracking susceptibility of these alloys.



Recent research has demonstrated particles such as carbides, oxides, and nitrides can act as hydrogen trapping sites⁵. Permanent hydrogen trapping sites can reduce the overall amount of diffusible hydrogen available to embrittle the metal, and can therefore reduce the cracking susceptibility of the alloy. The effectiveness of microstructural features to trap hydrogen depends largely on the type of feature. For example, oxide inclusions are more effective trapping sites than dislocations, while carbides are even more effective than oxides at trapping free hydrogen. Although the size and number

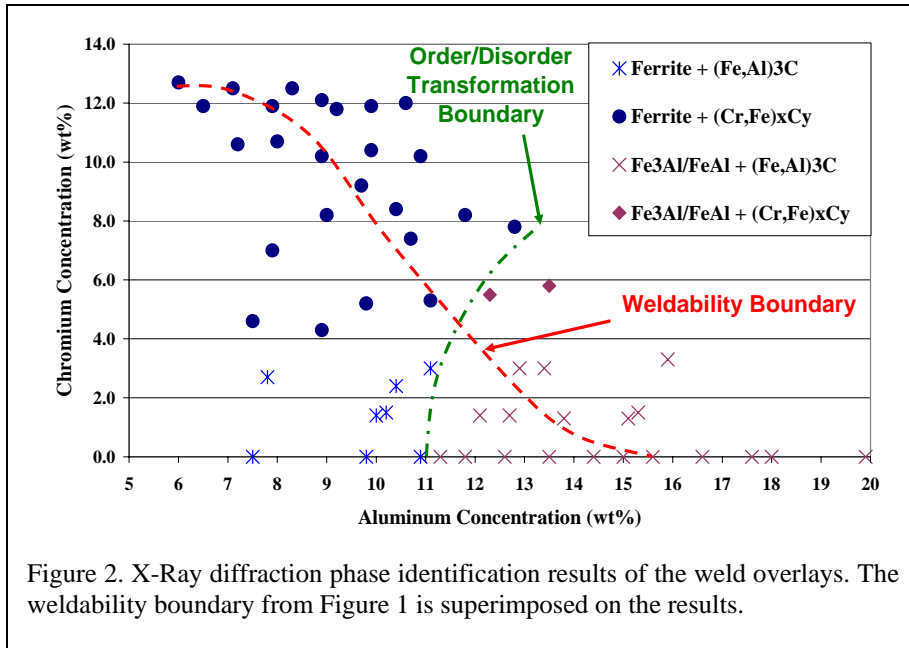


Figure 2. X-Ray diffraction phase identification results of the weld overlays. The weldability boundary from Figure 1 is superimposed on the results.

of particles within the welds are expected to effect the amount of trapped hydrogen, the amount of particle surface area within the weld should provide a more direct indication on the effectiveness of the particles to trap hydrogen. This is based on the idea that hydrogen trapping sites rely on the segregation of hydrogen to the particle/matrix interface, rather than hydrogen incorporation into the actual carbide or oxide⁵. Figure 3 shows that the particle surface area per unit volume of weld metal increases as the volume percent of particles increases, which is

expected. More importantly, the results indicate that the cracked and crack-free welds can be separated based on their particle surface area. For the current welding conditions, welds containing particle/matrix interfacial areas less than approximately $80 \text{ mm}^2/\text{mm}^3$ were susceptible to hydrogen cracking. Welds containing between approximately $80 \text{ mm}^2/\text{mm}^3$ and $100 \text{ mm}^2/\text{mm}^3$ particle surface area values appeared to undergo a transition between cracked and crack-free welds. Weld overlays containing particle surface areas greater than approximately $100 \text{ mm}^2/\text{mm}^3$ were found to be immune to hydrogen cracking. This correlation between the amount of particle surface area and the susceptibility of the welds to hydrogen cracking indicates that the size and distribution of particles within the weld has a significant effect on the hydrogen cracking behavior of the Fe-Cr-Al weld overlay claddings. It should be noted that the amount of surface area required to prevent cracking is expected to depend on the particle type, amount of hydrogen available, and residual stress. Thus, the results presented here are not intended to provide a general value required to prevent cracking, but to demonstrate the important role of particles in reducing the cracking susceptibility of these alloys. These results are described in more detail in Reference 6.

The results described above suggest that the carbon content of the weld should influence the amount of carbides in the weld and the corresponding resistance to hydrogen cracking. The cracking results of welds made on the low carbon substrates shown in Figure 4 confirm this expected trend. The weldability limit for the high carbon substrate is provided with these results for comparison. There is a rather distinct compositional boundary between welds that were cracked and crack-free for each substrate. These results show that a reduction in carbon content associated with the lower carbon substrate significantly decreases the range of weldable compositions. The difference in

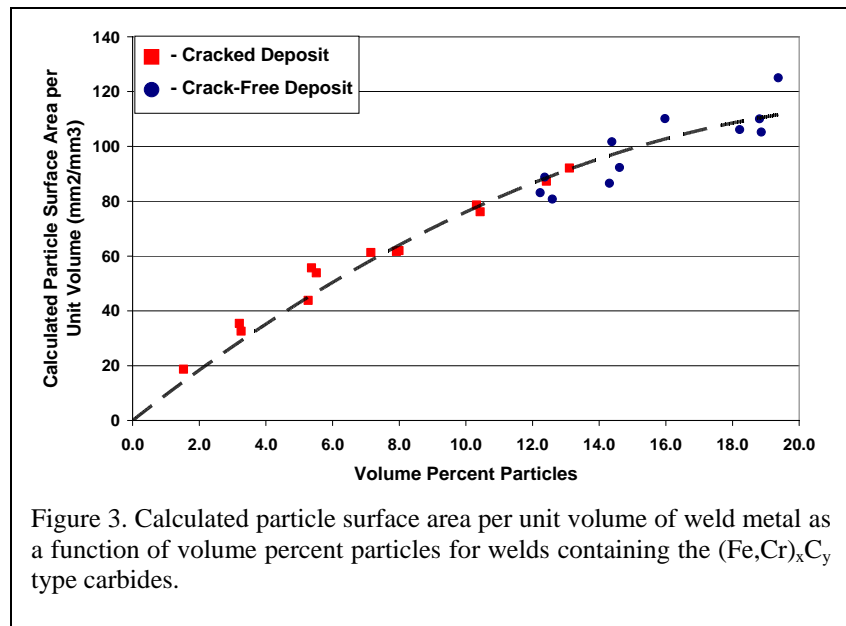
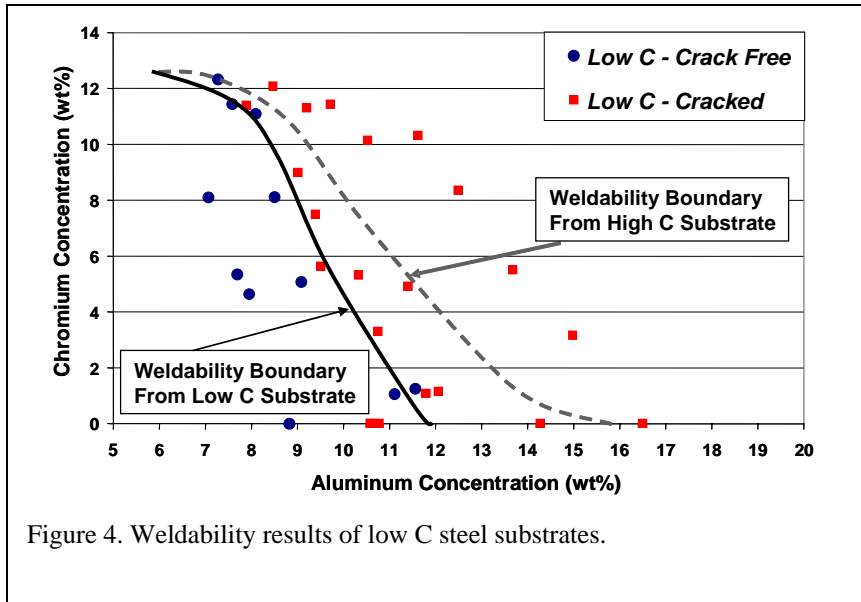


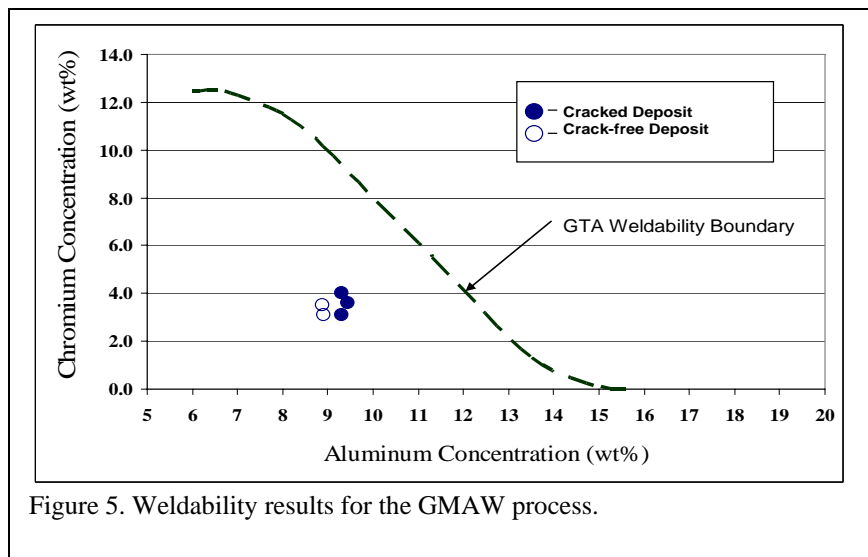
Figure 3. Calculated particle surface area per unit volume of weld metal as a function of volume percent particles for welds containing the $(\text{Fe,Cr})_x\text{C}_y$ type carbides.



cracking behavior between the low and high carbon welds is most significant at the lower chromium levels where the intermetallic phases form. Volume fraction measurements made on select samples confirmed that the amount of carbides in welds made on the low carbon substrate was much lower than those made on the high carbon substrate. For example, a 10.2Al-5.3Cr overlay made on the low carbon substrate contained only ~1 volume percent of particles and cracked, whereas a 9.8Al-5.2Cr overlay (i.e., similar Al and Cr) on the higher carbon steel plate contained ~15 volume percent particles and was crack-free.

GMA WELDS

Figure 5 shows typical weldability results for the GMA welds. The weldability boundary for the GTA welds is superimposed for reference. These results show that weld overlays prepared with the GMAW process can not tolerate as much Al and Cr before cracking occurs compared to the GTA weld overlays. GMA welds prepared under a wide range of conditions with different shielding gases and wire compositions showed similar results. This difference is attributed to the higher amount of hydrogen generally present with the GMAW process, which may be due to hydrogen pick up in the arc by the fine metal droplets transferred across the arc. Since GMAW is the preferred process for industrial applications due to the higher deposition rate, these results indicate that the weldability of these alloys needs to be improved so that higher Al and Cr concentrations can be accommodated for adequate corrosion resistance.



PRELIMINARY RESULTS ON TiC ADDITIONS

The GTA weldability results demonstrated that carbide particles can serve as effective hydrogen trapping sites for improving the cracking resistance, while the GMA results indicate that improvement in cracking resistance is needed in order to apply these alloys with the GMA process that is preferred by industry. Research conducted to date on the addition of hydrogen trap sites has shown that TiC is one of the most effective hydrogen trap sites due to its high binding energy⁵. The addition of TiC is also convenient for this system because TiC forms during solidification by a monovariant eutectic reaction during solidification. Thus, work has been initiated on a systematic study for controlled additions of TiC to these alloys for improved weldability. The amount of TiC that forms will depend on the amount of Ti and C, the solute redistribution behavior of Ti and C during solidification, and the

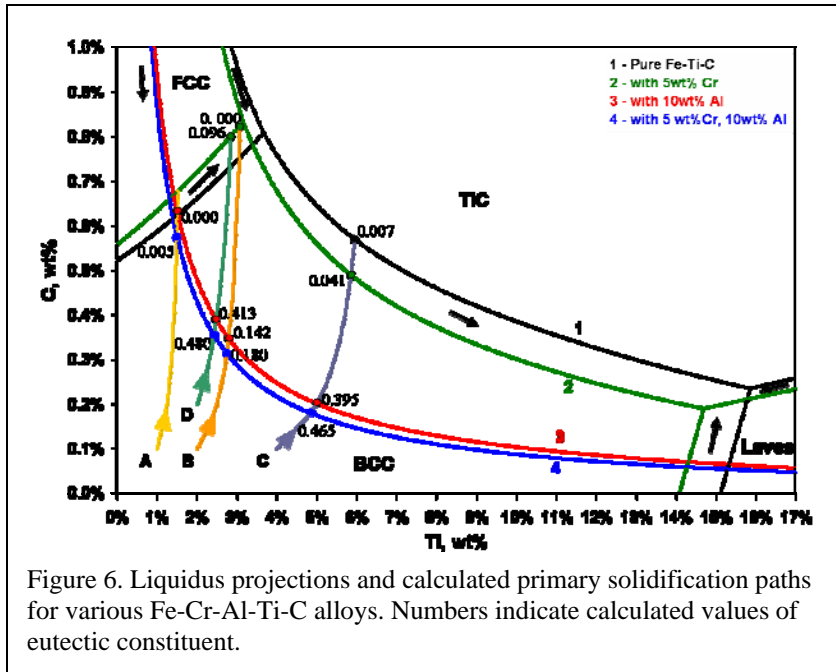


Figure 6. Liquidus projections and calculated primary solidification paths for various Fe-Cr-Al-Ti-C alloys. Numbers indicate calculated values of eutectic constituent.

amount of α -bcc / TiC eutectic that are expected to form during solidification are shown in Figure 6. The solute redistribution behavior was determined to be consistent with equilibrium solidification using Clyne and Kurz model⁸. The solidification paths and resultant amount of TiC-containing eutectic that forms was calculated using a solute redistribution model recently published⁷. The results indicate that the addition of 5wt% Cr to the Fe-Ti-C system, as in alloy system 2, caused the α /TiC mono-variant line to decrease to lower titanium and carbon concentrations, the α / γ -fcc mono-variant line increased to greater carbon concentrations, and the α /Laves mono-variant line decreased to lower titanium concentrations. The addition of 10wt% Al to the Fe-Ti-C system, as in alloy system 3, caused the α /TiC mono-variant line to decrease to much lower titanium and carbon concentrations than in alloy system 2, the α / γ mono-variant line increased to much greater carbon concentrations and is off the scale of the figure, and the α /Laves mono-variant line was not observed in the calculations which were conducted up to 20wt% Ti. The addition of 10wt% Al and 5wt% Cr to the Fe-Ti-C system, as in alloy system 4, caused the α /TiC boundary to decrease to even lower titanium and carbon concentrations than in alloy system 3, the α / γ boundary increases to even greater carbon concentrations and is again off the scale of the figure, and the α /Laves boundary was again not observed in the calculations performed up to 20wt% Ti. For each alloy system, the primary solidification path ends once it intersects the mono-variant eutectic line in its respective alloy system. The total fraction of eutectic that is expected to form for each alloy that intersects the mono-variant line is given next to the small dots in Figure 6. The fraction of eutectic that is expected to form provides an indication of how much TiC will form. The total fraction of eutectic that forms directly after primary solidification is equivalent to the fraction of liquid that remains when the primary solidification path intersects a mono-variant eutectic line. As 5wt% Cr is added to the Fe-Ti-C system, as in alloy C in system 2, the α /TiC monovariant line shifts to slightly lower Ti and C compositions. Thus, for identical Ti and C nominal compositions in the Fe-Ti-C and Fe-5Cr-Ti-C systems, the calculated primary solidification paths is truncated. This leads to a larger calculated fraction of liquid remaining when the solidification path intersects the mono-variant eutectic line and it would be expected that a higher volume fraction of monovariant eutectic α /TiC constituent will form. The same rational holds for the addition of 10wt% Al and 10wt%Al – 5wt%Cr to the Fe-Ti-C system, which both respectively further suppress the α /TiC monovariant line to lower Ti and C compositions. Alternatively, for a nominal composition increase of either or both Ti and C, the fraction of liquid present when the primary solidification path intersects the α /TiC mono-variant eutectic lines increases, which translates to an increasing amount of eutectic that should form. It appears that alloys B and D in system 2 come close to the triple point between fcc, bcc, and TiC phase fields. This may or may not occur depending on whether alloys actually solidify under absolute equilibrium conditions or if the positions of the calculated liquidus lines are completely accurate. The amount of TiC will also increase with additions of Ti and C, which is intuitively expected.

position of the monovariant eutectic lines on the appropriate liquidus projection⁷. A preliminary matrix of 16 alloys (Table 1) was prepared using arc button melting with systematic variations in Al, Cr, Ti, and C. The appropriate liquidus projections for the Fe-Ti-C, Fe-5Cr-Ti-C, Fe-10Al-Ti-C, and Fe-10Al-5Cr-Ti-C systems were calculated using Thermo-Calc. The 10Al and 5Cr levels are used here because these alloy levels have been shown to provide good corrosion resistance in a wide range of environments. The 10Al and 5Cr concentrations were added individually to the Fe-Ti-C system to observe the effect of TiC formation.

The calculated liquidus projections, primary solidification paths, and

Figure 7 compares preliminary results of the microstructures of Alloys 2B and 2D. The microstructures contain a α /TiC eutectic constituent in an α matrix. As expected, alloys from the “D” series exhibit significantly higher amounts of the α /TiC eutectic constituent due to the higher Ti and C additions. Work is in progress to quantify the amount of eutectic constituent in each alloy in order to validate the modeling results. This will provide a framework for controlling the amount of TiC in the alloy. Once this is accomplished, hydrogen desorption and weldability tests will be conducted to determine the effectiveness of the TiC additions for improving weldability.

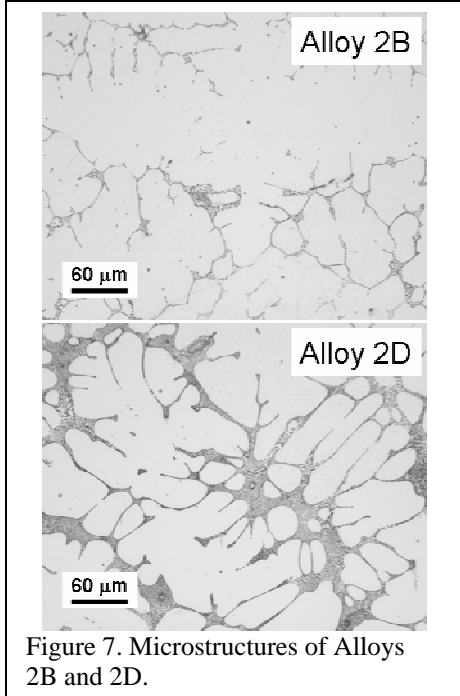


Figure 7. Microstructures of Alloys 2B and 2D.

Table 1: Compositions (wt %) of experimental Fe-Al-Cr-Ti-C alloys.

Alloy #	Fe	Al (wt%)	Cr (wt%)	Ti (wt%)	C (wt%)
1A	Balance	-	-	1	0.1
1B	Balance	-	-	2	0.1
1C	Balance	-	-	4	0.1
1D	Balance	-	-	2	0.2
2A	Balance	-	5	1	0.1
2B	Balance	-	5	2	0.1
2C	Balance	-	5	4	0.1
2D	Balance	-	5	2	0.2
3A	Balance	10	-	1	0.1
3B	Balance	10	-	2	0.1
3C	Balance	10	-	4	0.1
3D	Balance	10	-	2	0.2
4A	Balance	10	5	1	0.1
4B	Balance	10	5	2	0.1
4C	Balance	10	5	4	0.1
4D	Balance	10	5	2	0.2

CONCLUSIONS

The weldability and microstructure of Fe-Cr-Al weld overlays deposited onto carbon steel substrates was investigated. Work has also been initiated for improving the weldability of Fe-Cr-Al overlays through TiC additions. Results acquired to date show that cracking susceptibility is a strong function of the aluminum and chromium content of weld overlay. Additions of chromium to Fe-Al weld overlays will decrease the amount of aluminum that can be accommodated in the overlay before cracking begins to occur. The hydrogen cracking susceptibility of the Fe-Cr-Al welds can not be linked exclusively to the formation of the inherently brittle intermetallic compounds (Fe₃Al and FeAl). The presence of (Cr,Fe)_xC_y and (Fe,Al)₃C carbides significantly affected the cracking behavior of the welds, as high amounts of these carbides prevented hydrogen cracking in samples containing the intermetallic compounds. Additions of Ti and C to Fe-Cr-Al alloys leads to the formation of a microstructure with an α /TiC eutectic type constituent in an α matrix. The amount of α /TiC constituent is expected to increase with increasing Ti, C, Al, and Cr.

ACKNOWLEDGEMENTS

The authors gratefully acknowledge financial support of this research by the Fossil Energy Advanced Research and Technology Development Materials program, U.S. Department of Energy, under contract DE-AC05-96OR22464 with U.T. Battelle. The authors also gratefully acknowledge useful technical discussions with Dr. Peter Tortorelli from Oak Ridge National Laboratory.

REFERENCES

1. J. R. Regina, J. N. DuPont, and A. R. Marder, Gaseous Corrosion Resistance of Fe-Al Based Alloys Containing Cr Additions. Part I – Kinetic Results. *Accepted for Publication - Mat. Sci. and Eng. , A* (2004).
2. J. R. Regina, J. N. DuPont, and A. R. Marder, Corrosion Behavior of Fe-Al-Cr Alloys in Sulfur- and Oxygen-Rich Environments in the Presence of Pyrite. *Corrosion* **60**, 501-509 (2004).
3. S. W. Banovic, J. N. DuPont, P. F. Tortorelli, and A. R. Marder, The role of aluminum on the weldability and sulfidation behavior of iron-aluminum cladding. *Weld. Res. (Miami)* **78**, 23S-30S (1999).
4. M.G. Mendiratta, S.K. Ehlers, D.K. Chatterjee, and H.A. Lipsitt, Tensile flow and fracture behavior of DO3 iron-25 at% aluminum and iron-31at% aluminum alloys, *Metallurgical and Materials Transactions A*, 18A, (1987, pp. 283-291.
5. I. Maroef, D. L. Olson, M. Eberthart, and G. R. Edwards, Hydrogen trapping in ferritic steel weld metal. *International Materials Reviews* **47**, 191-223 (2002).
6. J. Regina, J.N. DuPont, and A.R. Marder, The Effect of Chromium on the Weldability and Microstructure of FeCrAl Weld Claddings, accepted for publication in *Welding Journal*.
7. J.N. DuPont, Mathematical Modeling of Solidification Paths in Ternary Alloys: Limiting Cases of Solute Redistribution, *Metallurgical and Materials Transactions A*, Vol 37A, June, 2006, pp. 1937-1947.
8. T.W. Clyne and W. Kurz, *Metallurgical Transactions A*, 1981; 12A: p. 965